NANO LETTERS

pubs.acs.org/NanoLett

Letter

Terahertz Spin-Conductance Spectroscopy: Probing Coherent and Incoherent Ultrafast Spin Tunneling

Reza Rouzegar,* Mohamed Amine Wahada, Alexander L. Chekhov, Wolfgang Hoppe, Genaro Bierhance, Jiří Jechumtál, Lukáš Nádvorník, Martin Wolf, Tom S. Seifert, Stuart S. P. Parkin, Georg Woltersdorf, Piet W. Brouwer, and Tobias Kampfrath

Cite This: *Nano Lett.* 2024, 24, 7852−7860

Read Online

ACCESS | Metrics & More | Article Recommendations | Supporting Information

ABSTRACT: Thin-film stacks $\mathcal{F}|\mathcal{H}$ consisting of a ferromagnetic-metal layer $\mathcal{F}$ and a heavy-metal layer $\mathcal{H}$ are spintronic model systems. Here, we present a method to measure the ultrabroadband spin conductance across a layer $\mathcal{X}$ between $\mathcal{F}$ and $\mathcal{H}$ at terahertz frequencies, which are the natural frequencies of spin-transport dynamics. We apply our approach to MgO tunneling barriers with thickness d = 0-6 Å. In the time domain, the spin conductance G_s has two components. An instantaneous feature arises from processes like coherent spin tunneling. Remarkably, a longer-lived component is a hallmark of incoherent resonant spin tunneling mediated by MgO defect states, because its relaxation time grows monotonically with d to as much as 270 fs at d = 6.0 Å. Our results are in full agreement with an analytical model. They indicate that terahertz spin-conductance spectroscopy will yield new and relevant insights into ultrafast spin transport in a wide range of spintronic nanostructures.

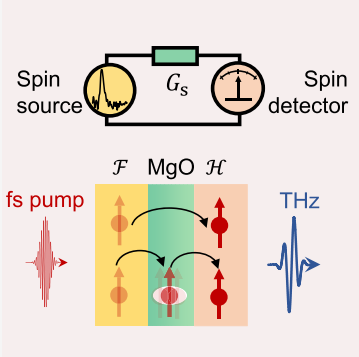

KEYWORDS: *Terahertz spintronics, spin conductance, terahertz spectroscopy, MgO tunnel junctions, coherent tunneling, incoherent resonant tunneling*

■ MOTIVATION

Transport of spin angular momentum by electrons is of central importance for future spintronic devices. To keep pace with other information carriers such as electronic charges in field-effect transistors[1] and photons in optical fibers,[2] spin transport needs to be pushed to terahertz (THz) bandwidth and, thus, femtosecond time scales. Promising applications of ultrafast spin currents include the generation of spin torque[3] for ultrafast magnetization switching and of broadband THz pulses[4,5] for spectroscopy.

In nanometer-thin $\mathcal{F}|\mathcal{H}$ stacks consisting of a ferromagnetic-metal layer $\mathcal{F}$ and a heavy-metal layer $\mathcal{H}$, THz spin transport from $\mathcal{F}$ to $\mathcal{H}$ can straightforwardly be driven by excitation with a femtosecond laser pulse.[4,6,7] The resulting spin current $j_s(t)$ vs time t can be characterized by conversion into a charge current in $\mathcal{H}$ and monitoring of the concomitantly emitted THz electromagnetic field. However, the measured THz signal $S = S(t)$ is connected to j_s by a complex response function, whose determination is not straightforward.[4,6,8] Even if the temporal evolution of j_s can be inferred from S, it is still convoluted with the dynamics of the force driving the spin current. Consequently, many THz-emission works do not consider the dynamics of $j_s(t)$ and rather focus on the peak amplitude, delay and bandwidth of THz signals.[5,9−14]

To characterize THz spin transport independently of the shape of driving force and setup transfer function, we borrow concepts from sub-THz spintronics. Here, an important quantity is the spin conductance $G_s = j_s/\Delta\mu_s$ which quantifies how much spin-current density j_s is obtained when a spin-voltage drop $\Delta\mu_s$ is applied across a conductor $\mathcal{X}$ (Figure 1a-c). We focus on longitudinal spin transport, which can be described by populations of spin-up and spin-down electron states. At frequencies up to 1 GHz, spin-transport measurements typically rely on electrical contacts.[15−17] At THz frequencies, however, measurement procedures of G_s still need to be developed.

In this work, we introduce an approach to measure the spin conductance of a thin film $\mathcal{X}$ between a ferromagnetic metal layer $\mathcal{F}$ and a heavy-metal layer $\mathcal{H}$ (Figure 1d). By using THz-emission spectroscopy,[18] we obtain the complex-valued spin conductance $\tilde{G}_s(\omega)$ at frequencies $\omega/2\pi$ = 0.5-12 THz. In the time domain, $G_s(t)$ vs time t can easily be understood as the spin current that would be obtained for a $\delta(t)$-like spin-voltage

Received: January 29, 2024
Revised: June 10, 2024
Accepted: June 11, 2024
Published: June 21, 2024

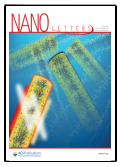

https://doi.org/10.1021/acs.nanolett.4c00498
Nano Lett. 2024, 24, 7852−7860

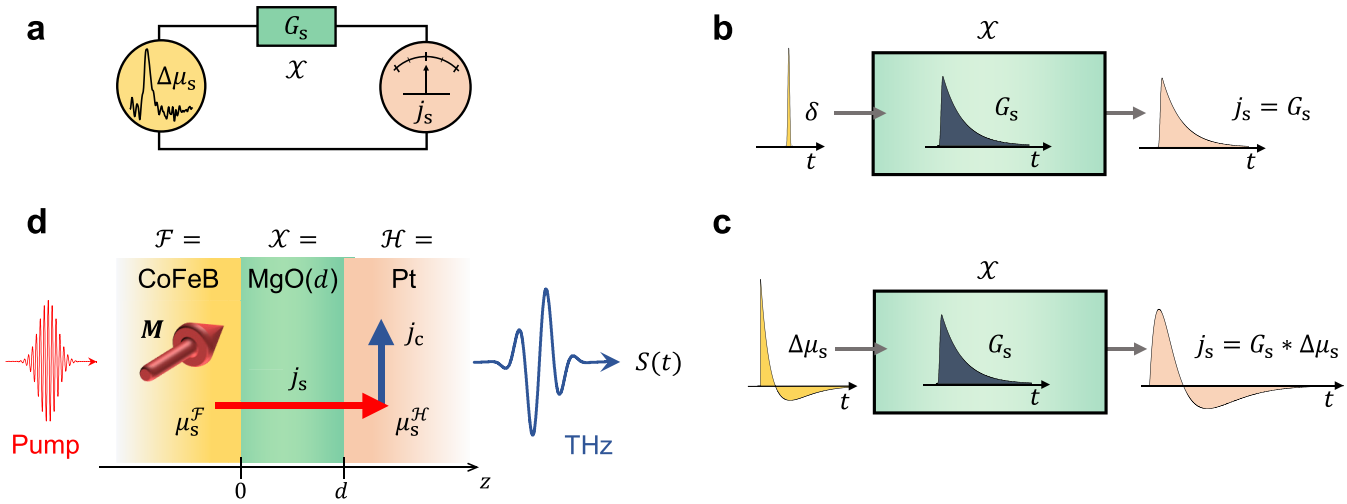

Figure 1. Spin-conductance spectroscopy of a layer $\mathcal{X}$ at terahertz frequencies. (a) Schematic of the concept. A transient spin voltage $\Delta\mu_s$ vs time t is applied across a spin conductor $\mathcal{X}$. The resulting spin-current density j_s is measured by a suitable detector and scales linearly with $\Delta\mu_s$ and the spin conductance G_s of $\mathcal{X}$. (b) The dynamics of $G_s = G_s(t)$ with time t can simply be understood as the spin current $j_s(t)$ that is obtained for an impulsive spin voltage $\Delta\mu_s(t) \propto \delta(t)$. (c) For arbitrary spin-voltage dynamics $\Delta\mu_s(t)$, the spin current is given by the convolution $j_s = G_s * \Delta\mu_s$ (eq 1). By Fourier transformation into the frequency domain, the convolution turns into a simple multiplication $\tilde{j}_s(\omega) = \tilde{G}_s(\omega)\Delta\tilde{\mu}_s(\omega)$, which can be solved for the spin conductance $\tilde{G}_s(\omega)$ at each frequency $\omega/2\pi$. (d) In the experiment, a thin layer $\mathcal{X}$ of MgO in a $\mathcal{F}|\mathcal{X}|\mathcal{H}$ thin-film stack is studied, where the ferromagnetic layer $\mathcal{F}$ = CoFeB and a heavy-metal layer $\mathcal{H}$ = Pt serve as spin-current source and detector, respectively. A femtosecond laser pulse induces a transient spin voltage $\mu_s^{\mathcal{F}}$ in $\mathcal{F}$ and, thus, spin transport through $\mathcal{X}$. The spin current j_s arriving in $\mathcal{H}$ is converted into an in-plane charge current $j_c(t) \propto j_s(t)$ and detected by sampling the THz pulse that j_c emits. By using the measured THz signal $S(t)$ and eq 3, we determine G_s for various $\mathcal{X}$ thicknesses d.

pulse. Our procedure is successfully demonstrated for a tunnel barrier $\mathcal{X}$ made of MgO and reveals dynamic signatures of coherent and incoherent spin tunneling. We expect that THz spin-conductance spectroscopy will provide important insights into ultrafast spin transport in a wide range of materials.

THZ SPIN-CONDUCTANCE SPECTROSCOPY

The general idea of spin-conductance spectroscopy is shown in Figure 1a. A spin voltage $\Delta\mu_s$ across spin conductor $\mathcal{X}$ drives a spin current j_s through $\mathcal{X}$. Importantly, the response of $\mathcal{X}$ is often linear and can, therefore, be fully quantified by applying an impulsive spin voltage $\Delta\mu_s(t) = \delta(t)$ (Figure 1b). The resulting spin current $j_s(t) = G_s(t)$ is known as the spin conductance of $\mathcal{X}$ in the time domain. It is an example of an impulse-response function, which is a very intuitive concept. For example, any response $G_s(t > 0)$ after the excitation at $t = 0$ points to memory effects like the storage and release of spins by $\mathcal{X}$ (Figure 1b).

In a typical experiment, however, the spin-voltage dynamics $\Delta\mu_s(t)$ is not impulsive (Figure 1c). In this general case, the resulting spin current is given by the convolution

$$j_s(t) = (G_s * \Delta\mu_s)(t) = \int \mathrm{d}u\, G_s(t-u)\, \Delta\mu_s(u) \tag{1}$$

of G_s and $\Delta\mu_s$ in the time domain. Eq 1 turns into the simple multiplication

$$\tilde{j}_s(\omega) = \tilde{G}_s(\omega)\Delta\tilde{\mu}_s(\omega) \tag{2}$$

in the frequency domain, where the tilde denotes Fourier transformation. Therefore, even for a nonimpulsive spin voltage, eq 2 allows us to obtain the spin conductance $\tilde{G}_s(\omega)$ over the frequency bandwidth of $\Delta\tilde{\mu}_s$.

To push this concept to THz frequencies, we employ a $\mathcal{F}|\mathcal{X}|\mathcal{H}$ stack (Figure 1d). The metallic ferromagnetic layer $\mathcal{F}$ (here CoFeB) serves as spin-current source, $\mathcal{X}$ is the layer under investigation, and the heavy-metal layer $\mathcal{H}$ (here Pt) acts as detector. First, a femtosecond laser pulse instantaneously heats the electrons in $\mathcal{F}$. The resulting excess of spin density in $\mathcal{F}$, also known as generalized spin voltage[7,19] $\mu_s^{\mathcal{F}}(t)$ of $\mathcal{F}$, drives a spin current through $\mathcal{X}$. Second, the spin current $j_s(t)$ arriving in $\mathcal{H}$ = Pt is converted into an in-plane charge current with density $j_c(t) \propto j_s(t)$ by the inverse spin Hall effect (ISHE). Third, $j_c(t)$ gives rise to the emission of a measurable ultrashort THz electromagnetic pulse that is probed by electro-optic sampling, resulting in a signal waveform $S(t)$ (Figure 1d).[4,6]

To infer G_s from the signals S, we take the following steps, as rationalized in Supporting Notes 1-3. First, a possible spin voltage $\mu_s^{\mathcal{H}}$ in $\mathcal{H}$ = Pt plays a minor role, that is, $\Delta\mu_s = \mu_s^{\mathcal{F}} - \mu_s^{\mathcal{H}} = \mu_s^{\mathcal{F}}$. Second, to determine $\mu_s^{\mathcal{F}}$, we conduct a reference measurement on a sample without interlayer $\mathcal{X}$, where $\tilde{j}_s^{\mathrm{ref}}(\omega) = \tilde{G}^{\mathrm{ref}}(\omega)\tilde{\mu}_s^{\mathcal{F}}(\omega)$ with known $\tilde{G}^{\mathrm{ref}}(\omega)$ (eq 2). Third, $\tilde{S}$ and $\tilde{j}_s$ are related by a response function that greatly cancels when the reference measurement is considered.[8] Consequently, the spin conductance $\tilde{G}_s$ of $\mathcal{X}$, normalized to the reference conductance $\tilde{G}^{\mathrm{ref}}(\omega)$, is fully and simply determined by the observables $\tilde{S}$ and $\tilde{S}^{\mathrm{ref}}$ through

$$\frac{\tilde{G}_s(\omega)}{g_0^{\mathrm{ref}}} = \frac{\tilde{j}_s(\omega)}{\tilde{j}_s^{\mathrm{ref}}(\omega)} = \frac{\tilde{S}(\omega)}{\tilde{S}^{\mathrm{ref}}(\omega)} \tag{3}$$

In the last step of eq 3, we took advantage of the facts that the measured optical absorptance and THz impedance of all the samples in our experiment are the same and, thus, cancel, and that the spin conductance $\tilde{G}^{\mathrm{ref}}(\omega) = g_0^{\mathrm{ref}}$ of the $\mathcal{F}|\mathcal{H}$ interface

https://doi.org/10.1021/acs.nanolett.4c00498
Nano Lett. 2024, 24, 7852−7860

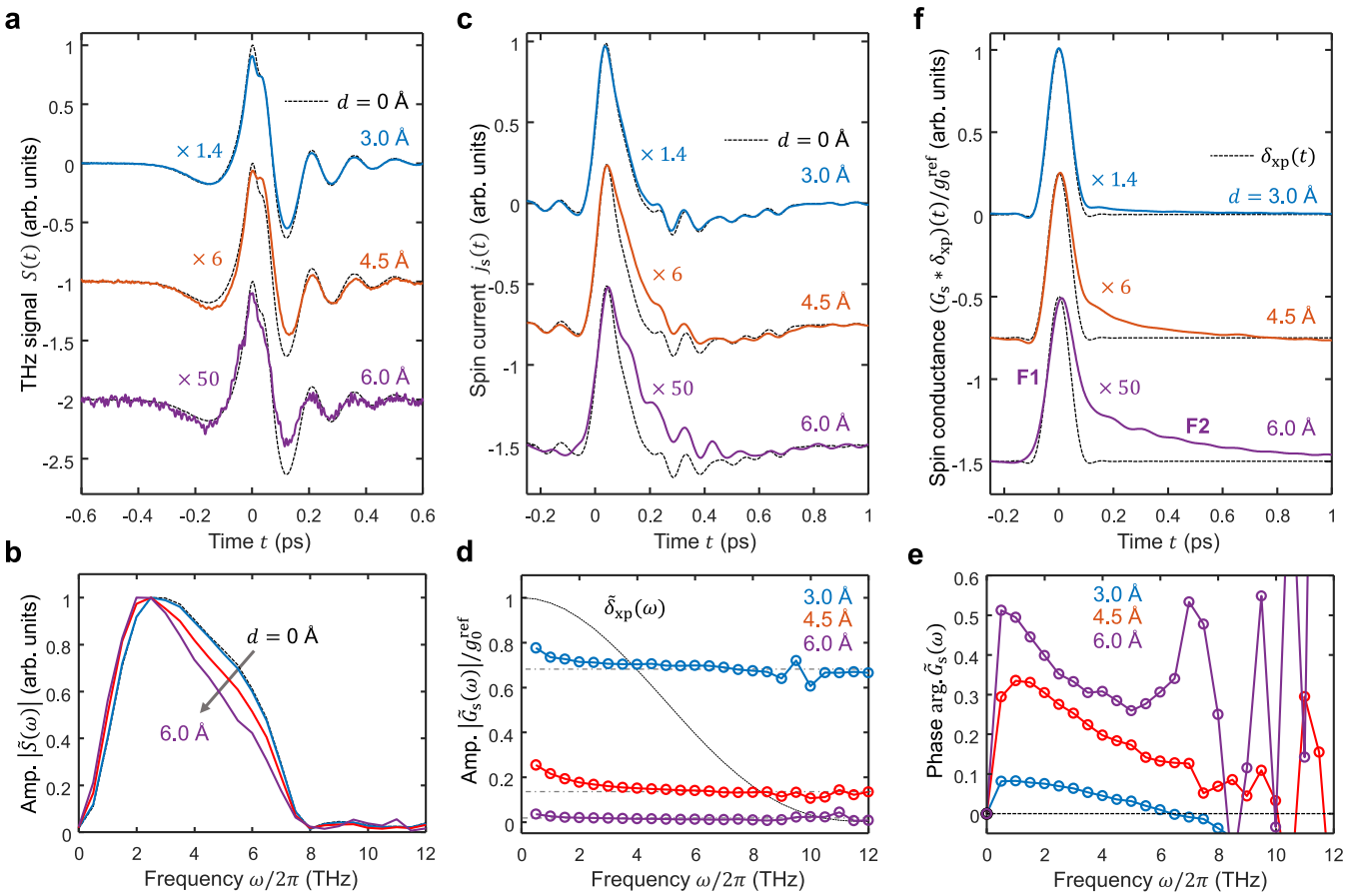

Figure 2. From THz signals to spin currents to spin conductance for CoFeB(2 nm)|MgO(d)|Pt(2 nm). (a) Time-domain electro-optic THz signals $S(t)$ odd in the CoFeB magnetization $\boldsymbol{M}$ for various MgO thicknesses of d = 0, 3.0, 4.5, and 6.0 Å. The signal for d = 0 is the reference signal $S^{ref} = S|_{d=0}$ (dashed lines). (b) Fourier amplitude spectra of the signals shown in panel (a). Maxima are normalized to unity. (c) Spin current $j_s(t)$ extracted from the THz signals shown in panel (a). The dashed lines correspond to $j_s(t)|_{d=0} \propto \mu_s^{\mathcal{F}}(t)$ (d) Amplitude of the frequency-domain spin conductance $|\tilde{G}_s(\omega)/g_0^{ref}|$ vs frequency $\omega/2\pi$, where $g_0^{ref} = \tilde{G}_s(\omega)|_{d=0}$ is found to be ω-independent. The function $\tilde{\delta}_{xp}(\omega)$ (dashed black line) indicates the finite frequency bandwidth of our setup. (e) Spectral phase arg $\tilde{G}_s(\omega)$. (f) Time-domain THz spin conductance of MgO barriers with various thicknesses d (thin solid lines). Due to the nonzero time resolution, the δ-function is broadened to a fictitious impulsive spin voltage $\delta_{xp}(t)$ (dashed lines), which equals the inversely Fourier-transformed $\tilde{\delta}_{xp}(\omega)$ in panel (e). Accordingly, the extracted conductivity curves are also broadened and display $(G_s * \delta_{xp})(t)$. For clarity, curves in panels (a, c, f) are offset vertically.

is constant over the frequency interval considered here (see Supporting Notes 1-3).

■ EXPERIMENTAL DETAILS

To put the scheme of Figure 1d to the test, we apply it to the nonmagnetic insulator $\mathcal{X}$ = MgO as a function of its thickness d. MgO has been extensively used as a tunnel barrier in magnetic tunnel junctions that provide large tunneling magnetoresistance for applications in nonvolatile memory devices.[20−23] The samples are

$$\text{substrate} \parallel \text{TaN}(1.5\text{nm})|\mathcal{F}(2\text{nm})|\mathcal{X}(d)|\mathcal{H}(2\text{nm})|\text{TaN}(1.5\text{nm})$$

stacks with $\mathcal{F}$ = CoFeB, various MgO thicknesses of $0 \leq d \leq 15$ Å and $\mathcal{H}$ = Pt. The sample with d = 0 is the reference sample without $\mathcal{X}$. All layers are grown on MgO substrates by DC magnetron sputtering at a base pressure of 4×10^{-3} mbar, except the MgO layer, which is grown in the same vacuum chamber by radio frequency sputtering using an off-axis gun tilted by 90° from the substrate plane.[11] Atomic-force microscopy shows a roughness of <2 Å for all layers.[11]

In the THz-emission experiments (Figure 1d), the magnetization $\boldsymbol{M}$ of $\mathcal{F}$ = CoFeB is saturated by an external magnetic field of about 10 mT parallel to the sample surface and perpendicular to the surface of the optical table. The sample is excited by a train of linearly polarized ultrashort laser pulses (central wavelength 790 nm, nominal pulse duration 10 fs, pulse energy 2 nJ, repetition rate 80 MHz) from a Ti:sapphire laser oscillator. The beam is normally incident onto the sample from the substrate side, traverses the substrate and arrives at the $\mathcal{F}|\mathcal{X}|\mathcal{H}$ stack with a focus size of 30 μm full width of half-maximum (FWHM) of intensity. The THz pulse that is emitted from the stack toward the air side is collimated and refocused by two 90°-off-axis parabolic mirrors into an electro-optic GaP(110) crystal (thickness 250 μm). Here, the THz electric field is sampled by linearly polarized probe pulses (0.6 nJ) from the same laser. This procedure yields the THz signal $S(t,\boldsymbol{M})$, i.e., the THz-field-induced probe ellipticity, as a function of the delay t between probe and THz pulse.[7]

As we are primarily interested in the charge current $j_c(t) \propto j_s(t)$ arising from the spin current from $\mathcal{F}$ = CoFeB and the inverse spin Hall effect in $\mathcal{H}$ = Pt, we detect the THz electric-field component perpendicular to the $\mathcal{F}$ magnetization $\boldsymbol{M}$ and only consider signals odd in $\boldsymbol{M}$, i.e., $S(t) = [S(t,+\boldsymbol{M}) - S(t,-\boldsymbol{M})]/2$. Signal components even in $\boldsymbol{M}$ are minor. The origin of

https://doi.org/10.1021/acs.nanolett.4c00498
Nano Lett. 2024, 24, 7852−7860

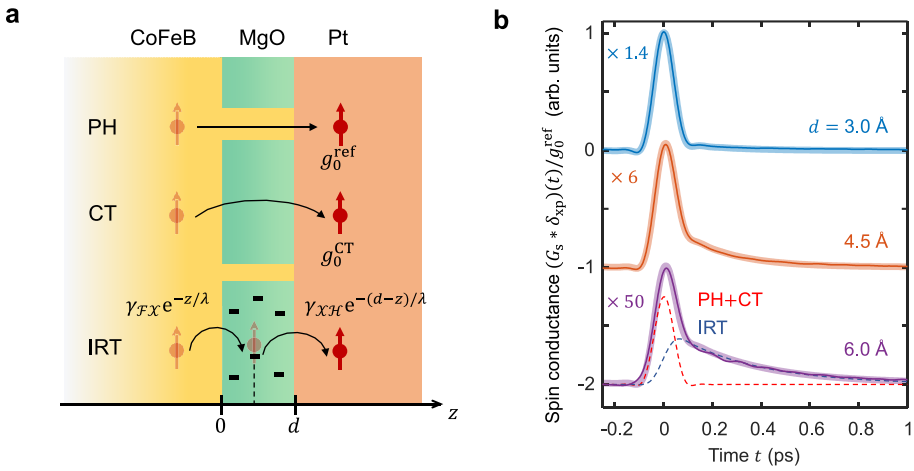

Figure 3. Interpretation of the THz spin conductances of MgO. (a) Spin-transport channels through MgO: flow through conducting pinholes (PH), coherent tunneling (CT), and incoherent resonant tunneling (IRT). For IRT, $\gamma_{\mathcal{FX}}e^{-z/\lambda}$ is the probability of an electron tunneling from $\mathcal{F}$ = CoFeB to a defect at position z in $\mathcal{X}$ = MgO, whereas $\gamma_{\mathcal{XH}}e^{-(d-z)/\lambda}$ is the tunneling probability from z to $\mathcal{H}$ = Pt. (b) Measured THz spin conductance (solid thin lines, from Figure 2f) along with fits (thick solid lines) based on eq 5. For d = 6 Å, the dashed lines show the instantaneous $[A\delta_{xp}(t)]$ and noninstantaneous $[B\Theta(t)e^{-t/\tau}]$ contribution, which is, respectively, ascribed to channels PH+CT (red dashed line) and IRT (blue dashed line).

the t axis may vary from sample to sample due, e.g., to variations of substrate thickness. Such shifts are typically <10 fs here and irrelevant, because we do not focus on possible d-dependent signal delays.[24]

THZ SIGNALS

Figures 2a and S1 show THz-emission signals $S(t)$ odd in $\boldsymbol{M}$ from CoFeB|MgO|Pt stacks for various MgO thicknesses d. The signal for d = 0 (Figure 2a) is dominated by ultrafast spin transport from CoFeB into Pt, where $\tilde{G}_s(\omega)|_{d=0} = g_0^{ref} = \text{const}_\omega$ (Supporting Note 4 and ref 7).

When d is increased from 0 to 6.0 Å, the signal amplitude decreases by a factor of 60 (Figure 2a). One can show that, in this range, the THz signal is dominated by spin transport from $\mathcal{F}$ through MgO into $\mathcal{H}$ and the ISHE in $\mathcal{H}$, consistent with the signal origin for d = 0. For d > 6.0 Å, the signals are increasingly superimposed by THz emission from layer $\mathcal{F}$ and, therefore, not considered further (see Supporting Note 4).

Interestingly, with increasing d, the signal amplitude drops, and the initially sharp temporal features become wider (Figure 2a). This trend suggests the emergence of slower components. It is confirmed by the normalized Fourier spectra (Figure 2b), whose width decreases with increasing d and whose maximum shifts to lower frequencies.

SPIN CURRENTS

By applying an inversion procedure to the signals in Figure 2a (see Supporting Note 1), we extract the spin-current dynamics $j_s(t)$ shown in Figure 2c. The spin current for the $\mathcal{F}|\mathcal{H}$ reference stack (d = 0, dashed line) has the same dynamics as the spin voltage of $\mathcal{F}$, i.e.,[7] $j_s(t) \propto \mu_s^{\mathcal{F}}(t)$. At arrival of the pump, $\mu_s^{\mathcal{F}}$ rises instantaneously, subsequently decreases with a rate given by the electron-spin relaxation time of CoFeB (≈100 fs), turns slightly negative and finally decays with a rate given by electron-phonon equilibration (≈400 fs).[7,25]

When the MgO thickness d increases from 0 to 6.0 Å, the amplitude of the spin current decreases, and its relaxation dynamics slows down (Figure 2c). For example, the $j_s(t)$ for d = 6.0 Å is 50 times smaller and relaxes substantially more slowly than the spin current measured in the reference sample (d = 0, dashed line).

FREQUENCY-DOMAIN SPIN CONDUCTANCE

Note that the spin currents $j_s = G_s * \mu_s^{\mathcal{F}}$ still contain the relatively complicated dynamics $\mu_s^{\mathcal{F}}(t)$ of the spin voltage (Figure 2c). To gain more intrinsic information on the dynamics of spin transport through MgO, we apply eq 3 to the raw signals (Figure 2a) in the frequency domain (Figure 2b) and determine the normalized spin conductance $\tilde{G}_s(\omega)/g_0^{ref}$ as a function of frequency $\omega/2\pi$ = 0.5-12 THz. We emphasize that this step does not require any knowledge of spin currents $j_s(t)$ nor transfer functions.

The modulus $|\tilde{G}_s(\omega)/g_0^{ref}|$ (Figure 2d) consists of a frequency-independent component (dashed-dotted lines) and an additional contribution below 3 THz. As expected from Figure 2a, we observe a drastic overall amplitude reduction with increasing d. At the same time, spectral weight is shifted to frequencies below 3 THz. The spectral phase arg $\tilde{G}_s(\omega)$ (Figure 2e) of the spin conductance and its slope vs ω increase with d, indicating an increasingly noninstantaneous response.

TIME-DOMAIN SPIN CONDUCTANCE

To obtain the time-domain spin conductance $G_s(t)$, one needs to inversely Fourier-transform $\tilde{G}_s(\omega)$. This task is not trivial because the Fourier amplitudes $\tilde{S}(\omega)$ of the THz signal are relatively small for frequencies $\omega/2\pi$ > 8 THz (Figure 2b). They are, thus, prone to unwanted signal contributions like noise, which lead to the strong random oscillations of the spectral phase arg $\tilde{G}_s(\omega)$ for $\omega/2\pi$ > 8 THz (Figure 2e).

To suppress these spectral components, we multiply $\tilde{G}_s$ with a suitable window function $\tilde{\delta}_{xp}$. The product $\tilde{G}_s\tilde{\delta}_{xp}$ in the frequency domain results in the convolution $G_s * \delta_{xp}$ of G_s with δ_{xp} in the time domain. To achieve a $\delta_{xp}(t)$ that is a single unipolar peak with a duration as short as possible, we use a Norton-Beer function[26,27] for $\tilde{\delta}_{xp}(\omega)$, which approaches zero at 12 THz (dashed line in Figure 2d). As a consequence, $G_s * \delta_{xp}$

https://doi.org/10.1021/acs.nanolett.4c00498
Nano Lett. 2024, 24, 7852−7860

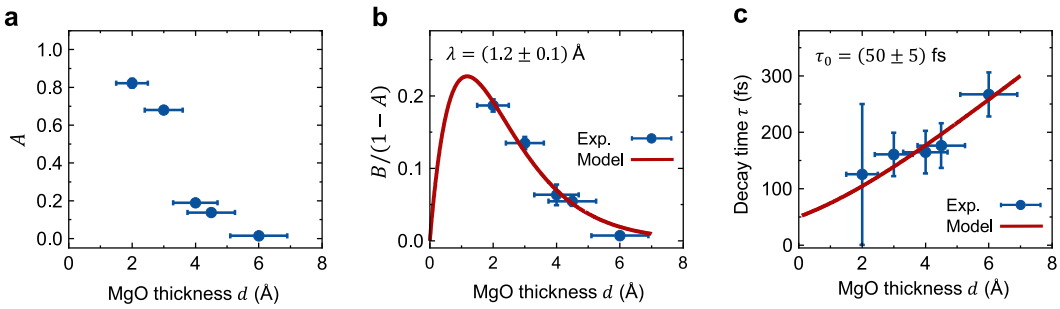

Figure 4. Parameters of the MgO spin conductance $G_s(t)$. (a) Amplitude $A \approx f^{PH}$ of the instantaneous, i.e., δ_{xp}-like component of G_s vs MgO thickness d (blue circles). (b) Amplitude $B/(1-A) \approx g_0^{IRT}/g_0^{ref}$ of the longer-lived G_s component vs MgO thickness (blue circles). The red solid line is a fit based on eq 7 with $\lambda = (1.2 \pm 0.1)$ Å. (c) Decay time τ of the IRT current component vs MgO thickness (blue circles). The red solid line is a fit based on eq 7 with $\tau_0 = (50 \pm 5)$ fs.

is a low-pass-filtered G_s, where possible sharp features are smeared over the width of δ_{xp} (dashed lines in Figure 2f). In other words, the 90 fs FWHM of $\delta_{xp}(t)$ defines the time resolution of the extracted $G_s(t)$.

The $G_s(t)$ traces (Figure 2f) consist of an initial instantaneous feature (F1) with a shape similar to $\delta_{xp}(t)$ and a subsequently tail-like feature (F2), whose relative weight increases with d. Component (F2) is fully consistent with the slower relaxation of the spin current $j_s(t)$ relative to the spin voltage $\mu_s^{\mathcal{F}}(t)$ (Figure 2c). However, the $G_s(t)$ traces much more clearly reveal that two features (F1) and (F2) generate the response of the MgO barrier. The reason is that the driving force of G_s, the fictitious impulsive spin voltage $\delta_{xp} \approx \delta$ (Figures 1b and 2f), has a much simpler structure than the experimental spin voltage $\mu_s^{\mathcal{F}}$ that induces the measured spin current j_s (Figures 1c and 2c).

Importantly, based on THz emission from samples tilted by ±45°, we estimate that possible pump-induced THz charge currents along the z axis (Figure 1d) are at least 2 orders of magnitude smaller than the in-plane currents j_c. Therefore, our extracted spin conductance $G_s(t)$ across $\mathcal{X}$ is measured under the boundary condition of negligible out-of-plane charge current.

■ INTERPRETATION

To interpret the dynamics of $G_s(t)$ (Figure 2f), we briefly review the relevant known static properties of MgO thin films. For d < 10 Å, structural imperfections are reported, in particular oxygen vacancies[28−33] and pinholes[34,35] connecting $\mathcal{F}$ and $\mathcal{H}$. Accordingly, we consider three possible contributions to the total spin current through MgO in CoFeB|MgO|Pt stacks (Figure 3a): spin transport through Pt- or CoFeB-filled pinholes (PH) in the MgO film,[35,36] coherent off-resonant electron tunneling (CT) through the MgO barrier[37−39] and incoherent resonant tunneling (IRT) through intermediate defect states in the vicinity of the Fermi energy of the CoFeB and Pt layer.[30,33,40−42] As the three channels PH, CT and IRT add up independently (Figure 3a), the spin conductance is the sum

$$G_s = G_s^{PH} + G_s^{CT} + G_s^{IRT} \tag{4}$$

While the PH and CT processes are instantaneous[7,43] on the time scale of our experimental resolution of 90 fs (dashed line in Figure 2f), the IRT mechanism may require more time to proceed.

To find analytic expressions for G_s^{PH}, G_s^{CT} and G_s^{IRT}, we discuss each mechanism in more detail. Regarding G_s^{PH}, one expects that, for d < 6 Å, MgO grows as islands[34] or exhibits pinholes.[35] The pinholes are filled with Pt of the subsequently grown Pt layer and, thus, provide a conductive channel between the CoFeB and Pt layer (Figure 3a). As G_s^{PH} is proportional to the in-plane areal pinhole fraction $0 \le f^{PH} \le 1$ and instantaneous, we model it by $G_s^{PH}(t) = f^{PH} g_0^{ref} \delta(t)$. Likewise, CT (Figure 3a) through the entire MgO barrier is instantaneous on the scale of our time resolution.[43] Therefore, $G_s^{CT}(t) = (1-f^{PH}) g_0^{CT} \delta(t)$, where g_0^{CT} is the amplitude of the impulsive spin current in the absence of pinholes.

Regarding IRT, oxygen vacancies are known to provide localized electronic states within the MgO band gap and, thus, open up a resonant transport channel.[28,31,32] In the simplest IRT model, an electron tunnels from $\mathcal{F}$ into a MgO vacancy and, subsequently, into $\mathcal{H}$ (Figure 3a), similarly to resonant tunneling in quantum wells.[44−47] One can quantify the resonant tunneling as $G_s^{IRT}(t) = (1-f^{PH}) g^{IRT}(t)$, where $g^{IRT}(t)$ is the IRT-related spin conductance of an MgO barrier without pinholes. Based on Figure 3a, we model $g^{IRT}(t)$ by a single-sided exponential decay $g_0^{IRT}\Theta(t)e^{-t/\tau}$, where $\Theta(t)$ is the Heaviside step function and τ can be considered as the characteristic time of IRT.

With these specifications, eq 4 turns into

$$\frac{G_s(t)}{g_0^{ref}} = A\delta(t) + B\Theta(t)e^{-t/\tau} \tag{5}$$

where

$$A = f^{PH} + (1 - f^{PH})\frac{g_0^{CT}}{g_0^{ref}},\ B = (1 - f^{PH})\frac{g_0^{IRT}}{g_0^{ref}} \tag{6}$$

We fit the convolution $G_s * \delta_{xp}$ of G_s (eq 5) with our time resolution δ_{xp} to the measured time-domain spin conductance (Figure 2f). Here, the free parameters are τ, A, B and a possible deviation t_0 from time zero, i.e., $t \to t - t_0$ in eq 5, due to substrate-thickness variations.[9] We find that $|t_0|$ is typically smaller than 10 fs (see Supporting Note 5).

The model fits (Figure 3b) describe our data excellently. The resulting amplitude A of the δ-like contribution (Figure 4a) decreases monotonically with MgO thickness d, where one can show that $A \approx f^{PH}$ (see Supporting Note 6). This assignment and Figure 4a are consistent with previous work[35] in which f^{PH} was found to decrease with increasing MgO thickness d on a scale of 2 Å. According to calculations,[11] MgO

https://doi.org/10.1021/acs.nanolett.4c00498
Nano Lett. 2024, 24, 7852−7860

layers close to the CoFeB and Pt interface are slightly metallic. They have a total thickness of about 4 Å and can be understood to have a large PH fraction. This effect may explain the pronounced drop of A when d is increased from 3.0 to4.0 Å (Figure 4a).

Using $A \approx f^{\mathrm{PH}}$, we can determine $g_0^{\mathrm{IRT}}/g_0^{\mathrm{ref}} \approx B/(1-A)$, i.e., the peak amplitude of the IRT contribution (eq 5), which is found to decrease strongly with increasing d (Figure 4b and Supporting Note 6). Remarkably, the characteristic IRT time τ is found to grow with d (Figure 4c), consistent with the increase of the slope of arg $\tilde{G}_s(\omega)$ vs ω (Figure 2e). As a side effect, the shape of $G_s(t)$ attains an asymmetry with increasing d that, after convolution with δ_{xp}, causes a shift of the peak of $G_s * \delta_{xp}$.

■ MODEL OF DYNAMIC IRT

Qualitatively, we suggest the following dynamic scenario for the IRT conductance $g^{\mathrm{IRT}}(t) \propto \Theta(t)\mathrm{e}^{-t/\tau}$. At time $t = 0$, a $\delta(t)$-like spin voltage in CoFeB drives instantaneous tunneling of spin-polarized electrons from CoFeB to MgO defect states (Figure 3a). Simultaneously, spin-unpolarized electrons are transferred from Pt to CoFeB to maintain local charge neutrality.

The subsequent tunneling events from occupied defect states to CoFeB or Pt are stochastic. Their rate $\partial N^{\sigma}/\partial t$ is proportional to the number N^{σ} of spins $\sigma = \uparrow$ or $\downarrow$ occupying the defect state. Accordingly, we obtain (i) a simple temporal exponential decay of N^{σ} and, thus, the σ-current from defects to Pt. (ii) The characteristic time of this process increases with increasing d because the tunneling from defects to Pt becomes less likely as d and, thus, the average distance of defect and Pt grow. As two tunneling events over distance d are involved, (iii) the spin current from CoFeB to Pt decreases with increasing d. The implications (i), (ii), (iii) of our model are fully consistent with the experimental results of Figures 3b, 4c and 4b, respectively.

More quantitatively, a rate-equation treatment and the assumption of vanishing out-of-plane charge current (see Supporting Note 7) reproduce the relationship $g^{\mathrm{IRT}}(t) = g_0^{\mathrm{IRT}}\Theta(t)\mathrm{e}^{-t/\tau}$ with

$$g_0^{\mathrm{IRT}} \propto d\mathrm{e}^{-d/\lambda},\ \tau = \tau_0 \frac{d/\lambda}{1-\mathrm{e}^{-d/\lambda}} \tag{7}$$

Here, τ_0 quantifies the spin lifetime in a defect state for an infinitely thin MgO layer with $d \ll \lambda$, where λ is the spin decay length in a MgO barrier. Eq 7 provides good fits to the data of Figure 4b, 4c and yields $\tau_0 = (50 \pm 5)$ fs and $\lambda = (1.2 \pm 0.1)$ Å, in agreement with previous measurements.[20,31,38,48,49]

■ DISCUSSION

The extracted λ value is up to 30% smaller than previously reported relaxation lengths[20,31,49] for at least two reasons. First, when d rises, the defect density in MgO is not constant but rather drops, resulting in an underestimation of λ. This effect may depend strongly on the MgO crystallinity[20,50,51] and could be addressed in future experiments. Second, the tunneling probability is spin-dependent with decay lengths[38] $\lambda^{\downarrow} < \lambda^{\uparrow}$. However, because no net charge is transported through MgO in our experiment, we measure the smaller $\lambda^{\downarrow}$, i.e., $\lambda \approx \lambda^{\downarrow}$ (see Supporting Note 7).

The spin-current relaxation time τ in defect states increases with the thickness of MgO, reaching as much as 270 fs for d = 6.0 Å. It is important to note that g_0^{IRT}, τ_0 and, thus, τ depend on the electron transparency of the $\mathcal{F}/\mathcal{H}$ and $\mathcal{X}/\mathcal{H}$ interfaces (see Supporting Note 7). Therefore, the magnitude and dynamics of the spin conductance $G_s(t)$ across a layer $\mathcal{X}$ depend not only on the bulk properties of $\mathcal{X}$, but also on its interfaces. However, the main characteristics of the IRT-based spin conductance of MgO remain unchanged: the spin decay length λ and the increase of the relaxation time τ with the MgO thickness. To gain more insight into the impact of the $\mathcal{F}/\mathcal{X}$ and $\mathcal{X}/\mathcal{H}$ interfaces on $g^{\mathrm{IRT}}(t)$, future studies may measure the THz spin conductance of MgO barriers as a function of the $\mathcal{F}$ and $\mathcal{H}$ material.

We emphasize that determination of the THz spin conductance (Figure 2f) relies on the measurement of just two THz emission signals (eq 3), without having to know any instrument response functions, in contrast to extraction of the spin current j_s (Figure 2c). This approach can be extended to, in principle, any $\mathcal{X}$ material other than MgO, if the following three assumptions are fulfilled: (A1) The signal exclusively arises from the spin current j_s arriving in $\mathcal{H}$. (A2) The j_s solely originates from the spin voltage $\Delta\mu_s = \mu_s^{\mathcal{F}} - \mu_s^{\mathcal{H}}$ and is dominated by $\mu_s^{\mathcal{F}}$. (A3) The presence of the layers $\mathcal{X}$ and $\mathcal{H}$ in the stack $\mathcal{F}|\mathcal{X}|\mathcal{H}$ does not change the dynamics of $\mu_s^{\mathcal{F}}$.

For our CoFeB|MgO(d)|Pt system, (A1) is fulfilled for the reference sample (d = 0), but also for $d \leq 6$ Å because the ISHE of Pt dominates spin-to-charge conversion of the metal stack (Supporting Note 4). (A2) is valid for the reference sample[7] and, thus, for $d \neq 0$, too (Supporting Note 3). (A3) is fulfilled for the reference sample (Supporting Note 3) and, thus, for $d > 0$ also. If layer $\mathcal{X}$ changes the pump absorptance and THz conductivity of the sample stack, their effect needs to be accounted for in eq 3 (Supporting Note 2). We again emphasize that the spin conductance determined with our approach (Figure 1d) refers to a situation with negligible net charge transport.

In conclusion, we demonstrate a new method, THz spin-conductance spectroscopy, to study ultrafast spin transport across a layer $\mathcal{X}$. We apply it to the example of MgO barriers and find an ultrafast signature of IRT: a spin-current relaxation tail whose decay time increases with the barrier thickness because the tunneling probability decreases. Our method inherits all benefits of THz-emission spectroscopy,[18,52−56] in particular contact-free operation with large sample throughput. Future work may push the time resolution down to the 10 fs scale of electron-momentum relaxation.[57,58] In this way, THz spin-conductance spectroscopy will provide significant means to separate elementary transport processes from ballistic to diffusive in a wide range of spintronic nanostructures made of simple metals[59] or complex materials like antiferromagnets.[60−62]

■ ASSOCIATED CONTENT

Supporting Information

The Supporting Information is available free of charge at https://pubs.acs.org/doi/10.1021/acs.nanolett.4c00498.

Supporting Figure S1: THz emission signals for CoFeB(3 nm)|MgO(d)|Pt(3 nm) with $0 \leq d \leq 15$ Å. Supporting Figure S2: THz emission from $\mathcal{F}|\mathcal{H}$ vs $\mathcal{F}$ samples. Supporting Note 1: Extraction of spin current from THz signals. Supporting Note 2: THz spin conductance of layer $\mathcal{X}$. Supporting Note 3: Spin

https://doi.org/10.1021/acs.nanolett.4c00498
Nano Lett. 2024, 24, 7852−7860

conductance of the CoFeB/Pt interface and Pt spin voltage. Supporting Note 4: Prevalence of spin transport from CoFeB to Pt for $d \leq 6$ Å. Supporting Note 5: Fitting by eq 5. Supporting Note 6: Analysis of A and eq 6. Supporting Note 7: Rate-equation model of IRT. (PDF)

AUTHOR INFORMATION

Corresponding Author

Reza Rouzegar − *Department of Physics, Freie Universität Berlin, 14195 Berlin, Germany; Department of Physical Chemistry, Fritz Haber Institute of the Max Planck Society, 14195 Berlin, Germany;* orcid.org/0000-0002-3171-2196; Email: m.rouzegar@fu-berlin.de

Authors

Mohamed Amine Wahada − *Max Planck Institute for Microstructure Physics, 06120 Halle, Germany; Institut für Physik, Martin-Luther-Universität Halle, 06120 Halle, Germany*

Alexander L. Chekhov − *Department of Physics, Freie Universität Berlin, 14195 Berlin, Germany; Department of Physical Chemistry, Fritz Haber Institute of the Max Planck Society, 14195 Berlin, Germany*

Wolfgang Hoppe − *Institut für Physik, Martin-Luther-Universität Halle, 06120 Halle, Germany*

Genaro Bierhance − *Department of Physics, Freie Universität Berlin, 14195 Berlin, Germany; Department of Physical Chemistry, Fritz Haber Institute of the Max Planck Society, 14195 Berlin, Germany;* orcid.org/0000-0002-1016-3570

Jiří Jechumtál − *Faculty of Mathematics and Physics, Charles University, 121 16 Prague, Czech Republic*

Lukáš Nádvorník − *Faculty of Mathematics and Physics, Charles University, 121 16 Prague, Czech Republic*

Martin Wolf − *Department of Physical Chemistry, Fritz Haber Institute of the Max Planck Society, 14195 Berlin, Germany*

Tom S. Seifert − *Department of Physics, Freie Universität Berlin, 14195 Berlin, Germany*

Stuart S. P. Parkin − *Max Planck Institute for Microstructure Physics, 06120 Halle, Germany;* orcid.org/0000-0003-4702-6139

Georg Woltersdorf − *Institut für Physik, Martin-Luther-Universität Halle, 06120 Halle, Germany;* orcid.org/0000-0001-9299-8880

Piet W. Brouwer − *Department of Physics, Freie Universität Berlin, 14195 Berlin, Germany*

Tobias Kampfrath − *Department of Physics, Freie Universität Berlin, 14195 Berlin, Germany; Department of Physical Chemistry, Fritz Haber Institute of the Max Planck Society, 14195 Berlin, Germany*

Complete contact information is available at: https://pubs.acs.org/10.1021/acs.nanolett.4c00498

Notes

The authors declare no competing financial interest.

ACKNOWLEDGMENTS

Financial support from the German research foundation (DFG) through the collaborative research center CRC/TRR 227 (project ID 328545488, projects A05, B02, B03, B05 and B10) is gratefully acknowledged. R.R. also acknowledges support by the International Max Planck Research School (IMPRS) for Elementary Processes in Physical Chemistry.

REFERENCES

(1) del Alamo, J. A. Nanometre-scale electronics with III−V compound semiconductors. *Nature* **2011**, *479* (7373), 317−323.

(2) Hillerkuss, D.; Schmogrow, R.; Schellinger, T.; Jordan, M.; Winter, M.; Huber, G.; Vallaitis, T.; Bonk, R.; Kleinow, P.; Frey, F.; Roeger, M.; Koenig, S.; Ludwig, A.; Marculescu, A.; Li, J.; Hoh, M.; Dreschmann, M.; Meyer, J.; Ben Ezra, S.; Narkiss, N.; Nebendahl, B.; Parmigiani, F.; Petropoulos, P.; Resan, B.; Oehler, A.; Weingarten, K.; Ellermeyer, T.; Lutz, J.; Moeller, M.; Huebner, M.; Becker, J.; Koos, C.; Freude, W.; Leuthold, J. 26 Tbit s−1 line-rate super-channel transmission utilizing all-optical fast Fourier transform processing. *Nat. Photonics* **2011**, *5* (6), 364−371.

(3) Kirilyuk, A.; Kimel, A. V.; Rasing, T. Ultrafast optical manipulation of magnetic order. *Rev. Mod. Phys.* **2010**, *82* (3), 2731−2784.

(4) Kampfrath, T.; Battiato, M.; Maldonado, P.; Eilers, G.; Nötzold, J.; Mährlein, S.; Zbarsky, V.; Freimuth, F.; Mokrousov, Y.; Blügel, S.; Wolf, M.; Radu, I.; Oppeneer, P. M.; Münzenberg, M. Terahertz spin current pulses controlled by magnetic heterostructures. *Nat. Nanotechnol.* **2013**, *8* (4), 256−260.

(5) Zhou, C.; Liu, Y. P.; Wang, Z.; Ma, S. J.; Jia, M. W.; Wu, R. Q.; Zhou, L.; Zhang, W.; Liu, M. K.; Wu, Y. Z.; Qi, J. Broadband Terahertz Generation via the Interface Inverse Rashba-Edelstein Effect. *Phys. Rev. Lett.* **2018**, *121* (8), No. 086801.

(6) Seifert, T.; Jaiswal, S.; Martens, U.; Hannegan, J.; Braun, L.; Maldonado, P.; Freimuth, F.; Kronenberg, A.; Henrizi, J.; Radu, I.; Beaurepaire, E.; Mokrousov, Y.; Oppeneer, P. M.; Jourdan, M.; Jakob, G.; Turchinovich, D.; Hayden, L. M.; Wolf, M.; Münzenberg, M.; Kläui, M.; Kampfrath, T. Efficient metallic spintronic emitters of ultrabroadband terahertz radiation. *Nat. Photonics* **2016**, *10* (7), 483−488.

(7) Rouzegar, R.; Brandt, L.; Nádvorník, L.; Reiss, D. A.; Chekhov, A. L.; Gueckstock, O.; In, C.; Wolf, M.; Seifert, T. S.; Brouwer, P. W.; Woltersdorf, G.; Kampfrath, T. Laser-induced terahertz spin transport in magnetic nanostructures arises from the same force as ultrafast demagnetization. *Phys. Rev. B* **2022**, *106* (14), No. 144427.

(8) Seifert, T. S.; Jaiswal, S.; Barker, J.; Weber, S. T.; Razdolski, I.; Cramer, J.; Gueckstock, O.; Maehrlein, S. F.; Nadvornik, L.; Watanabe, S.; Ciccarelli, C.; Melnikov, A.; Jakob, G.; Münzenberg, M.; Goennenwein, S. T. B.; Woltersdorf, G.; Rethfeld, B.; Brouwer, P. W.; Wolf, M.; Kläui, M.; Kampfrath, T. Femtosecond formation dynamics of the spin Seebeck effect revealed by terahertz spectroscopy. *Nat. Commun.* **2018**, *9* (1), 2899.

(9) Seifert, T. S.; Tran, N. M.; Gueckstock, O.; Rouzegar, S. M.; Nadvornik, L.; Jaiswal, S.; Jakob, G.; Temnov, V. V.; Münzenberg, M.; Wolf, M.; Kläui, M.; Kampfrath, T. *Terahertz spectroscopy for all-optical spintronic characterization of the spin-Hall-effect metals Pt, W and Cu80Ir20. J. Phys. D: Appl. Phys.* **2018**, *51* (36), No. 364003.

(10) Gorchon, J.; Mangin, S.; Hehn, M.; Malinowski, G. Is terahertz emission a good probe of the spin current attenuation length? *Appl. Phys. Lett.* **2022**, *121* (1), 012402.

(11) Wahada, M. A.; Şaşıoğlu, E.; Hoppe, W.; Zhou, X.; Deniz, H.; Rouzegar, R.; Kampfrath, T.; Mertig, I.; Parkin, S. S. P.; Woltersdorf, G. Atomic Scale Control of Spin Current Transmission at Interfaces. *Nano Lett.* **2022**, *22* (9), 3539−3544.

(12) Schneider, R.; Fix, M.; Bensmann, J.; Michaelis de Vasconcellos, S.; Albrecht, M.; Bratschitsch, R. Spintronic GdFe/Pt THz emitters. *Appl. Phys. Lett.* **2019**, *115* (15), No. 152401.

(13) Kholid, F. N.; Hamara, D.; Hamdan, A. F. B.; Nava Antonio, G.; Bowen, R.; Petit, D.; Cowburn, R.; Pisarev, R. V.; Bossini, D.; Barker, J.; Ciccarelli, C. The importance of the interface for picosecond spin pumping in antiferromagnet-heavy metal heterostructures. *Nat. Commun.* **2023**, *14* (1), 538.

(14) Dang, T. H.; Hawecker, J.; Rongione, E.; Baez Flores, G.; To, D. Q.; Rojas-Sanchez, J. C.; Nong, H.; Mangeney, J.; Tignon, J.; Godel, F.; Collin, S.; Seneor, P.; Bibes, M.; Fert, A.; Anane, M.;

George, J.-M.; Vila, L.; Cosset-Cheneau, M.; Dolfi, D.; Lebrun, R.; Bortolotti, P.; Belashchenko, K.; Dhillon, S.; Jaffrès, H. Ultrafast spin-currents and charge conversion at 3d-5d interfaces probed by time-domain terahertz spectroscopy. *Applied Physics Reviews* **2020**, *7* (4), 041409.

(15) Bauer, G. E. W.; Saitoh, E.; van Wees, B. J. Spin caloritronics. *Nat. Mater.* **2012**, *11* (5), 391−399.

(16) Manchon, A.; Železný, J.; Miron, I. M.; Jungwirth, T.; Sinova, J.; Thiaville, A.; Garello, K.; Gambardella, P. Current-induced spin-orbit torques in ferromagnetic and antiferromagnetic systems. *Rev. Mod. Phys.* **2019**, *91* (3), No. 035004.

(17) Sinova, J.; Valenzuela, S. O.; Wunderlich, J.; Back, C. H.; Jungwirth, T. Spin Hall effects. *Rev. Mod. Phys.* **2015**, *87* (4), 1213−1260.

(18) Seifert, T. S.; Cheng, L.; Wei, Z.; Kampfrath, T.; Qi, J. Spintronic sources of ultrashort terahertz electromagnetic pulses. *Appl. Phys. Lett.* **2022**, *120* (18), No. 180401.

(19) Bierhance, G.; Markou, A.; Gueckstock, O.; Rouzegar, R.; Behovits, Y.; Chekhov, A. L.; Wolf, M.; Seifert, T. S.; Felser, C.; Kampfrath, T. Spin-voltage-driven efficient terahertz spin currents from the magnetic Weyl semimetals Co2MnGa and Co2MnAl. *Appl. Phys. Lett.* **2022**, *120* (8), No. 082401.

(20) Yuasa, S.; Djayaprawira, D. D. Giant tunnel magnetoresistance in magnetic tunnel junctions with a crystalline MgO(0 0 1) barrier. *J. Phys. D: Appl. Phys.* **2007**, *40* (21), R337.

(21) Apalkov, D.; Dieny, B.; Slaughter, J. M. Magnetoresistive random access memory. *Proceedings of the IEEE* **2016**, *104* (10), 1796−1830.

(22) Wang, L.; Cheng, H.; Li, P.; Van Hees, Y. L. W.; Liu, Y.; Cao, K.; Lavrijsen, R.; Lin, X.; Koopmans, B.; Zhao, W. Picosecond optospintronic tunnel junctions. *Proc. Natl. Acad. Sci. U. S. A.* **2022**, *119* (24), e2204732119.

(23) Jin, Z.; Li, J.; Zhang, W.; Guo, C.; Wan, C.; Han, X.; Cheng, Z.; Zhang, C.; Balakin, A. V.; Shkurinov, A. P.; Peng, Y.; Ma, G.; Zhu, Y.; Yao, J.; Zhuang, S. Magnetic Modulation of Terahertz Waves via Spin-Polarized Electron Tunneling Based on Magnetic Tunnel Junctions. *Physical Review Applied* **2020**, *14* (1), No. 014032.

(24) Jechumtál, J.; Rouzegar, R.; Gueckstock, O.; Denker, C.; Hoppe, W.; Remy, Q.; Seifert, T. S.; Kubaščík, P.; Woltersdorf, G.; Brouwer, P. W.; Münzenberg, M.; Kampfrath, T.; Nádvorník, L. Accessing Ultrafast Spin-Transport Dynamics in Copper Using Broadband Terahertz Spectroscopy. *Phys. Rev. Lett.* **2024**, *132* (22), No. 226703.

(25) Rouzegar, R.; Chekhov, A. L.; Behovits, Y.; Serrano, B. R.; Syskaki, M. A.; Lambert, C. H.; Engel, D.; Martens, U.; Münzenberg, M.; Wolf, M.; Jakob, G.; Kläui, M.; Seifert, T. S.; Kampfrath, T. *Broadband Spintronic Terahertz Source with Peak Electric Fields Exceeding 1.5 MV/cm*. *Physical Review Applied* **2023**, *19* (3), No. 034018.

(26) Chekhov, A. L.; Behovits, Y.; Heitz, J. J. F.; Denker, C.; Reiss, D. A.; Wolf, M.; Weinelt, M.; Brouwer, P. W.; Münzenberg, M.; Kampfrath, T. Ultrafast Demagnetization of Iron Induced by Optical versus Terahertz Pulses. *Physical Review X* **2021**, *11* (4), No. 041055.

(27) Naylor, D. A.; Tahic, M. K. Apodizing functions for Fourier transform spectroscopy. *J. Opt. Soc. Am. A* **2007**, *24* (11), 3644−3648.

(28) Mather, P. G.; Read, J. C.; Buhrman, R. A. *Disorder, defects, and band gaps in ultrathin (001) MgO tunnel barrier layers*. *Phys. Rev. B* **2006**, *73* (20), No. 205412.

(29) Cha, J. J.; Read, J. C.; Buhrman, R. A.; Muller, D. A. Spatially resolved electron energy-loss spectroscopy of electron-beam grown and sputtered CoFeB/MgO/CoFeB magnetic tunnel junctions. *Appl. Phys. Lett.* **2007**, *91* (6), No. 062516.

(30) Velev, J. P.; Belashchenko, K. D.; Jaswal, S. S.; Tsymbal, E. Y. Effect of oxygen vacancies on spin-dependent tunneling in Fe/MgO/Fe magnetic tunnel junctions. *Appl. Phys. Lett.* **2007**, *90* (7), No. 072502.

(31) Miao, G. X.; Park, Y. J.; Moodera, J. S.; Seibt, M.; Eilers, G.; Münzenberg, M. Disturbance of Tunneling Coherence by Oxygen Vacancy in Epitaxial $\mathrm{Fe}/\mathrm{MgO}/\mathrm{Fe}$ Magnetic Tunnel Junctions. *Phys. Rev. Lett.* **2008**, *100* (24), No. 246803.

(32) Ke, Y.; Xia, K.; Guo, H. Oxygen-Vacancy-Induced Diffusive Scattering in $\mathrm{Fe}/\mathrm{MgO}/\mathrm{Fe}$ Magnetic Tunnel Junctions. *Phys. Rev. Lett.* **2010**, *105* (23), No. 236801.

(33) Tsymbal, E. Y.; Pettifor, D. G. Local impurity-assisted conductance in magnetic tunnel junctions. *Phys. Rev. B* **2001**, *64* (21), No. 212401.

(34) König, T.; Simon, G. H.; Rust, H. P.; Heyde, M. Work Function Measurements of Thin Oxide Films on Metals—MgO on Ag(001). *J. Phys. Chem. C* **2009**, *113* (26), 11301−11305.

(35) Teixeira, J. M.; Ventura, J.; Carpinteiro, F.; Araujo, J. P.; Sousa, J. B.; Wisniowski, P.; Freitas, P. P. The effect of pinhole formation/growth on the tunnel magnetoresistance of MgO-based magnetic tunnel junctions. *J. Appl. Phys.* **2009**, *106* (7), No. 073707.

(36) König, T.; Simon, G. H.; Rust, H. P.; Pacchioni, G.; Heyde, M.; Freund, H. J. Measuring the Charge State of Point Defects on MgO/Ag(001). *J. Am. Chem. Soc.* **2009**, *131* (48), 17544−17545.

(37) Mathon, J.; Umerski, A. Theory of tunneling magnetoresistance of an epitaxial Fe/MgO/Fe(001) junction. *Phys. Rev. B* **2001**, *63* (22), No. 220403.

(38) Butler, W. H.; Zhang, X. G.; Schulthess, T. C.; MacLaren, J. M. Spin-dependent tunneling conductance of $\mathrm{Fe}|\mathrm{MgO}|\mathrm{Fe}$ sandwiches. *Phys. Rev. B* **2001**, *63* (5), No. 054416.

(39) Butler, W. H. Tunneling magnetoresistance from a symmetry filtering effect. *Sci. Technol. Adv. Mater.* **2008**, *9* (1), No. 014106.

(40) Velev, J. P.; Zhuravlev, M. Y.; Belashchenko, K. D.; Jaswal, S. S.; Tsymbal, E. Y.; Katayama, T.; Yuasa, S. Defect-Mediated Properties of Magnetic Tunnel Junctions. *IEEE Trans. Magn.* **2007**, *43* (6), 2770−2775.

(41) Gadzuk, J. W. Resonance Tunneling Through Impurity States in Metal-Insulator-Metal Junctions. *J. Appl. Phys.* **1970**, *41* (1), 286−291.

(42) Teixeira, J. M.; Ventura, J.; Araujo, J. P.; Sousa, J. B.; Wisniowski, P.; Cardoso, S.; Freitas, P. P. Resonant Tunneling through Electronic Trapping States in Thin MgO Magnetic Junctions. *Phys. Rev. Lett.* **2011**, *106* (19), 196601.

(43) Landsman, A. S.; Weger, M.; Maurer, J.; Boge, R.; Ludwig, A.; Heuser, S.; Cirelli, C.; Gallmann, L.; Keller, U. Ultrafast resolution of tunneling delay time. *Optica* **2014**, *1* (5), 343−349.

(44) Mathon, J.; Umerski, A. Theory of resonant tunneling in an epitaxialFe/Au/MgO/Au/Fe(001)junction. *Phys. Rev. B* **2005**, *71* (22), 220402.

(45) Yuasa, S.; Nagahama, T.; Suzuki, Y. Spin-Polarized Resonant Tunneling in Magnetic Tunnel Junctions. *Science* **2002**, *297* (5579), 234−237.

(46) Lu, Z.-Y.; Zhang, X. G.; Pantelides, S. T. Spin-Dependent Resonant Tunneling through Quantum-Well States in Magnetic Metallic Thin Films. *Phys. Rev. Lett.* **2005**, *94* (20), 207210.

(47) Glazov, M. M.; Alekseev, P. S.; Odnoblyudov, M. A.; Chistyakov, V. M.; Tarasenko, S. A.; Yassievich, I. N. Spin-dependent resonant tunneling in symmetrical double-barrier structures. *Phys. Rev. B* **2005**, *71* (15), No. 155313.

(48) Xu, Y.; Ephron, D.; Beasley, M. R. Directed inelastic hopping of electrons through metal-insulator-metal tunnel junctions. *Phys. Rev. B* **1995**, *52* (4), 2843−2859.

(49) Yuasa, S.; Nagahama, T.; Fukushima, A.; Suzuki, Y.; Ando, K. Giant room-temperature magnetoresistance in single-crystal Fe/MgO/Fe magnetic tunnel junctions. *Nat. Mater.* **2004**, *3* (12), 868−871.

(50) Mukherjee, S. S.; Bai, F.; MacMahon, D.; Lee, C.-L.; Gupta, S. K.; Kurinec, S. K. Crystallization and grain growth behavior of CoFeB and MgO layers in multilayer magnetic tunnel junctions. *J. Appl. Phys.* **2009**, *106* (3), No. 033906.

(51) Choi, Y. S.; Tsunekawa, K.; Nagamine, Y.; Djayaprawira, D. Transmission electron microscopy study on the polycrystalline CoFeB/MgO/CoFeB based magnetic tunnel junction showing a

high tunneling magnetoresistance, predicted in single crystal magnetic tunnel junction. *J. Appl. Phys.* **2007**, *101* (1), 013907.
(52) Papaioannou, E. T.; Beigang, R. THz spintronic emitters: a review on achievements and future challenges. *Nanophotonics* **2021**, *10* (4), 1243−1257.
(53) Feng, Z.; Qiu, H.; Wang, D.; Zhang, C.; Sun, S.; Jin, B.; Tan, W. Spintronic terahertz emitter. *J. Appl. Phys.* **2021**, *129* (1), 010901.
(54) Cheng, L.; Li, Z.; Zhao, D.; Chia, E. E. M. Studying spin−charge conversion using terahertz pulses. *APL Materials* **2021**, *9* (7), 070902.
(55) Bull, C.; Hewett, S. M.; Ji, R.; Lin, C.-H.; Thomson, T.; Graham, D. M.; Nutter, P. W. Spintronic terahertz emitters: Status and prospects from a materials perspective. *APL Materials* **2021**, *9* (9), 090701.
(56) Wu, W.; Yaw Ameyaw, C.; Doty, M. F.; Jungfleisch, M. B. Principles of spintronic THz emitters. *J. Appl. Phys.* **2021**, *130* (9), No. 091101.
(57) Krewer, K. L.; Zhang, W.; Arabski, J.; Schmerber, G.; Beaurepaire, E.; Bonn, M.; Turchinovich, D. Thickness-dependent electron momentum relaxation times in iron films. *Appl. Phys. Lett.* **2020**, *116* (10), 102406.
(58) Nádvorník, L.; Borchert, M.; Brandt, L.; Schlitz, R.; de Mare, K. A.; Výborný, K.; Mertig, I.; Jakob, G.; Kläui, M.; Goennenwein, S. T. B.; Wolf, M.; Woltersdorf, G.; Kampfrath, T. Broadband Terahertz Probes of Anisotropic Magnetoresistance Disentangle Extrinsic and Intrinsic Contributions. *Physical Review X* **2021**, *11* (2), No. 021030.
(59) Melnikov, A.; Brandt, L.; Liebing, N.; Ribow, M.; Mertig, I.; Woltersdorf, G. Ultrafast spin transport and control of spin current pulse shape in metallic multilayers. *Phys. Rev. B* **2022**, *106* (10), 104417.
(60) Lee, K.; Lee, D.-K.; Yang, D.; Mishra, R.; Kim, D.-J.; Liu, S.; Xiong, Q.; Kim, S. K.; Lee, K.-J.; Yang, H. Superluminal-like magnon propagation in antiferromagnetic NiO at nanoscale distances. *Nat. Nanotechnol.* **2021**, *16* (12), 1337−1341.
(61) Sasaki, Y.; Li, G.; Moriyama, T.; Ono, T.; Mikhaylovskiy, R. V.; Kimel, A. V.; Mizukami, S. Laser stimulated THz emission from Pt/CoO/FeCoB. *Appl. Phys. Lett.* **2020**, *117* (19), 192403.
(62) Gueckstock, O.; Seeger, R. L.; Seifert, T. S.; Auffret, S.; Gambarelli, S.; Kirchhof, J. N.; Bolotin, K. I.; Baltz, V.; Kampfrath, T.; Nádvorník, L. Impact of gigahertz and terahertz transport regimes on spin propagation and conversion in the antiferromagnet IrMn. *Appl. Phys. Lett.* **2022**, *120* (6), 062408.

https://doi.org/10.1021/acs.nanolett.4c00498
Nano Lett. 2024, 24, 7852−7860